

Image quality with non-standard nuclides in PET

R. LAFOREST, X. LIU

Non-standard positron emission tomography (PET) nuclides bring with them the prospect of new chemistry leading the way to novel approaches for targeted imaging and therapy. In particular, the kinetic energy of the positron of some of these nuclides is high (as much as 4 MeV) and, thus, a highly specific PET probe can be very lethal to cancerous cells. However, the high positron energy will degrade the spatial resolution, and this degradation will be more important in high-resolution, small animal PET imaging, where most of the novel tracers are developed. This paper discusses the image quality in small animal PET imaging obtained with such nuclides. The nuclides of ^{60}Cu , ^{61}Cu and ^{64}Cu , ^{76}Br , $^{94\text{m}}\text{Tc}$, and ^{89}Zr will be particularly analyzed. The spatial resolution will be seen to degrade with nuclides with higher positron end-point energy, going from 1.7 mm for ^{18}F to 2.2 mm for ^{76}Br , for example. Many of these novel PET nuclides decay by the emission of cascades γ rays that are detected in coincidence with the positron annihilation photons which create additional noise on the images. However, the use of an image reconstruction algorithm, which includes a model of the statistical nature of nuclear decay and the modeling of the tomograph response, contributes to both improve the spatial resolution and at the same time reduce the image noise.

KEY WORDS: Radionuclide imaging - Radiopharmaceuticals - Tomography, emission computed.

Funding.—This work was funded by the National Cancer Institute under the grant RadioNuclide Resource for Cancer Applications (RRCA, 1 R24CA86307) and from the US Department of Energy (DE-FG02-87ER60212).

Acknowledgments.—Special thanks go to L. Tang for the development of the engineering aspect of the phantoms and to the RRCA staff and cyclotron personnel for production and delivery of the activity.

Address reprint requests to: R. Laforest, Ph.D., Mallinckrodt Institute of Radiology, Washington University School of Medicine, 510 S. Kingshighway Blvd., Campus Box 8225, St. Louis, MO 63110, USA. E-mail: laforestr@wustl.edu

*Mallinckrodt Institute of Radiology
Washington University School of Medicine
St. Louis, MO, USA*

Positron emission tomography (PET) holds great promises for the advance of the understanding of human diseases and, furthermore, the use of small animal PET offers tremendous opportunities for translational research to the human arena. The development of PET radiotracers is a very active field of research for the development of radiotracers with uptake more specific to particular targets. The use of other PET nuclides, other than any of the four standard nuclides (^{11}C , ^{15}O , ^{13}N or ^{18}F) is an important new avenue of radiotracer research as it opens the possibility for development of novel chemistry leading to the exploration of novel targets with new probes. At Washington University in St. Louis, we have undertaken an impressive program for the production and distribution of non-standard PET nuclides in order to support this endeavor and provide nuclides that would not be available otherwise. A review of the production and utilization of some of these nuclides is presented in Schueller *et al.*¹ and Welch *et al.*² Most of these non-standard nuclides are not ideal, however, for PET imaging as they characterized by high positron maximum energy and also by the emission of several β -delayed γ rays. As a consequence, the spatial resolution that can be achieved with those nuclides is usually poor and moreover, the cascade γ rays contribute greatly to reduce quantitation accuracy and contribute to poor noise property in the PET images.

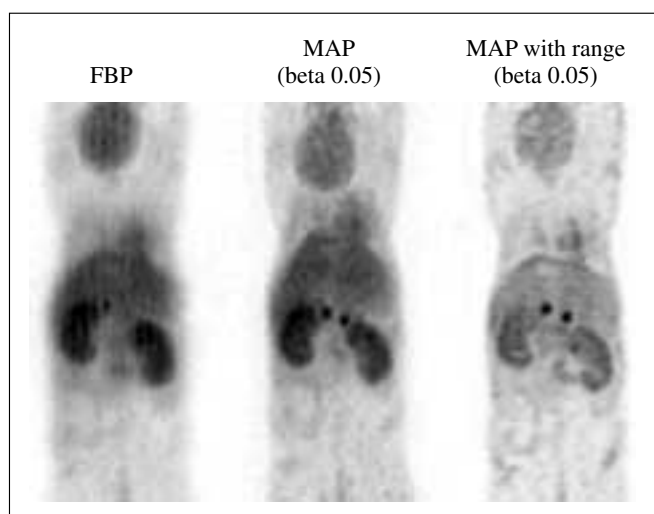


Figure 1.—Coronal images of a mouse injected with [^{61}Cu]PTSM and reconstructed with filtered back-projection (A), maximum *a posteriori* (MAP) (B) and MAP with positron range correction (C). The improved resolution provided by the resolution recovery algorithm of MAP is clearly visible, as well as the further improvement in resolution from the positron range correction.

In this report, we will discuss image quality issues when imaging by PET with non-standard nuclides. A special emphasis will be devoted to imaging in small animal imaging since the loss of resolution from the positron is most noticeable in high resolution imaging systems and, furthermore, most of the tracer development work is being done in small animal. The discussion will present results from imaging with the copper PET nuclides, ^{76}Br , $^{94\text{m}}\text{Tc}$ and ^{89}Zr , but similarly applicable conclusions can be reached for the other nuclides.

As an indication of the complexity of the decay scheme from those nuclides, the mean number of γ rays (including the annihilation photons) is substantially larger than two (*i.e.* for the two annihilation photons). For example in ^{60}Cu , ^{61}Cu , ^{76}Br and ^{86}Y , the average number of γ ray per decay is respectively 3.996, 2.18, 3.35 and 4.55. This means that, in average, there will be multiple possibilities to create coincidence pairs from the simultaneous detection of γ rays for each β decay event. The PET camera will be unable to discriminate among those which one is the true pair leading to useful image formation from fortuitous coincidences and, thus, images will be contaminated with these spurious counts. The images will consequently lose qualitative and quantitative accuracy.

Methods and results

Imaging with ^{60}Cu , ^{61}Cu and ^{64}Cu

The decay ^{60}Cu proceeds by the β^+ decay to a variety of excited states in the daughter ^{60}Ni nucleus. In particular, the decay branching ratio to the 3 MeV states is dominant and as a consequence the average β particle energy is lower than what it would be if the decay proceeds only to the daughter ground state. The maximum energy of the positron is >4 MeV which leads to positron range extending to >10 mm, however, due to the decay to excited states in ^{60}Ni , the positron range is strongly reduced albeit still being larger than for ^{61}Cu or ^{64}Cu . In Ruangma *et al.*,³ we have shown in phantom and in animal experiments that imaging with those nuclides in micro-PET can yield useful images. In particular, it could be noted from the imaging of a phantom containing a pattern of hot rods that 1.25 mm rods (separated by 6 mm) could be identified by PET using ^{60}Cu , which is surprising considering the long range of the positrons. This paper also reported on the use of a novel image reconstruction algorithm such as maximum *a posteriori* (MAP),⁴ which is an algorithm incorporating a model of the physical process of PET detection and the Poisson model of nuclear decay and photon counting. Higher image quality could be obtained with this algorithm, and in particular, the application of a positron range correction as part of the resolution recovery algorithm brought a noticeable improvement to image quality in these phantom experiments.

In animal studies,³ it was noted that for ^{60}Cu -, ^{61}Cu -, ^{64}Cu -labeled tracers injected in rats, images showed decreased resolution as compared to ^{61}Cu - or ^{64}Cu -labeled tracer, although the spatial resolution was still sufficient to identify all the bones including the vertebrae and all major organs. The use of MAP and of MAP plus the range correction allowed further improvement in spatial resolution even with long range emitter like ^{60}Cu . More similar images could be obtained when imaging is performed with ^{60}Cu , ^{61}Cu or ^{64}Cu with the use of MAP, or even MAP with a positron range correction. An example of the image reconstruction improvement with and MAP and MAP plus range is illustrated for [^{61}Cu]PTSM imaging in mice in Figure 1. Improved resolution from the resolution recovery capability of MAP and the further improvements brought by the positron range correction is illustrated.

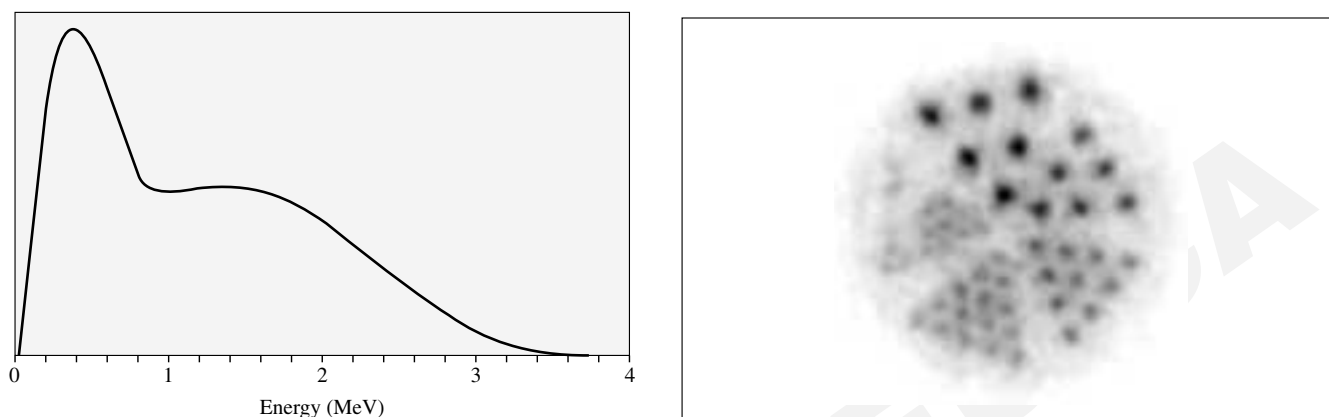


Figure 2.—A) Positron energy spectra from ^{76}Br depicting the low energy peak from the decay to the 3070 keV level in ^{76}Se ; B) a hot rod Derenzo phantom images with this nuclide showing the ability to identify 1 mm object in a high contrast situation despite the high energy tail of the positron spectra.

Imaging with ^{76}Br

Quantitative imaging in 2D and in human scanner with ^{76}Br has been previously studied in Beattie *et al.*⁵ and Lubberink *et al.*⁶ Bromine-76 decays at 56% by β^+ emission to various excited levels in ^{76}Se , the most dominant of which are a group of states around 3 MeV of excitation energy accounting for approximately 20% of the decays and to the 559 keV level (for 6% of the decay). This yield to the emission of the 559 keV γ rays with high yield (74%).^{7, 8} Similarly to the discussion the imaging with ^{60}Cu , the decay to excited states is beneficial for imaging resolution as the maximum energy of the positron is reduced by the excitation energy of the final states in the daughter nucleus. Due to this specific decay scheme, the positron energy spectra is characterized by a peak at relatively low energy and a second component extending to much higher energy (up to 3.9 MeV). The spectrum of β particle energies is presented in Figure 2A and shows the dominant peak at 0.4 MeV and the long high-energy positron energy tail. The low energy positrons will allow to achieve imaging with good spatial resolution, but since a substantial amount of β particles are emitted with high energy, the image contrast that can be obtained with this nuclide will still be low. This fact is illustrated in Figure 2B, which shows the imaging of a hot rod Derenzo phantom in a micro-PET-F120 with this nuclide. The phantom is composed of a pattern of 5 groups of fillable rods of diameter 2.5 mm, 2 mm, 1.5 mm, 1.25 mm and 1 mm separated by 4 times their diameter. We can note that

even the smallest rods can be distinguished although with reduced contrast, *i.e.* a flood of events appearing in between the rods.

A more thorough evaluation of the imaging performance of this nuclide was further performed by the imaging of a specially designed spatial resolution phantom consisting of two capillary tubes (250 μm internal diameter [ID]) immersed in a bath of water. The overall dimension of the phantom was 2.5 cm in diameter by 2.5 cm in length. The phantom was prepared by loading the capillary tubes and first image by surrounding the capillaries with non-radioactive water, and second by adding activity in the surrounding water so that the ratio of concentration was 300:1 relative to the capillaries and the uniform area. The same phantom was also imaged with similar condition with ^{18}F .

Image reconstruction was performed with standard 2D-filtered back-projection (FBP) and by MAP without the range correction. Images were reconstructed with various values of frequency cutoff parameter for the 2D-FBP reconstructions and for various values of the β factor, a factor in MAP controlling the smoothness in the images. Data were analyzed by extracting a line profile through the capillary tube image in a transverse plane and measuring the full width at half maximum (FWHM). Figure 3 shows these values of FWHM plotted as function of the frequency cutoff parameter or the β value for both imaging with ^{18}F and ^{76}Br .

FWHMs with ^{18}F are seen to be lower than with ^{76}Br due to the much lower positron range of ^{18}F , but,

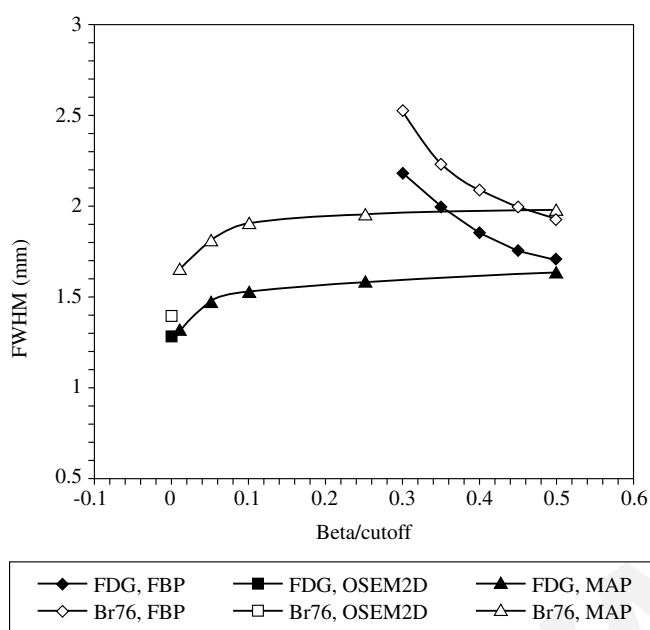


Figure 3.—Comparison of the achievable spatial resolution in a small animal positron emission tomography (PET) scanner between ^{18}F and ^{76}Br . A fine line source filled with activity was imaged in the micro-PET-F120 and images were reconstructed with filtered back-projection (FBP) and maximum *a posteriori* (MAP) with different value of frequency cut-off parameter for FBP and β value for MAP.

surprisingly, the FWHMs for ^{76}Br are just slightly higher than the ones with ^{18}F despite the very high-energy tail. FWHMs for ^{76}Br approaches 2.1 mm (1.7 mm with MAP) despite the high positron energy. For both nuclides, we can observe lower spatial resolution with 2D-FBP at 0.5cm^{-1} cutoff frequency (Nyquist frequency) and for the lower value of the β parameter. The relatively low value of the FWHM is interesting and explains the observations we made before that the smallest rods could be identified in Figure 2B.

However, the FWHM does not give a complete picture of the resolution capability of this nuclide. The long tail of positron energy yields to positrons with a long range and as a consequence, the full width at tenth of the maximum is much larger than what would be obtained from a short-range positron emitter. A closer inspection of the line spread function measured with this phantom reveals that a good fit of the profile can be obtained by fitting a double Gaussian distribution, one with a narrow width (~ 2 mm) and a second much larger one (~ 6.4 mm). Accurate determination of this function is important as it allows

determination of the point spread function for this nuclide, which in turn can be used to recover quantitation accuracy.

NOISE CHARACTERISTICS

As indicated before, the presence of cascade γ rays results in a decrease of counting rate capability from this nuclide. In particular, the 559 keV γ ray (74% yield) is detected with a similar detection efficiency as the annihilation photons and thus contribute to the generation of a uniform background of counts in sinogram space. In this work, the subtraction of the cascade background component is performed by a uniform background subtraction as reported in Bigott *et al.*⁹ The net effect of larger positron range and the presence and subtraction of cascade coincidences is expected to increase the noise in the images. To quantify this aspect, a uniform phantom containing a 1 cm diameter fillable sphere immerse in a fillable uniform cylinder (3 cm ID, 5 cm long) was imaged with ^{76}Br and with ^{18}F as a comparison by preparing the phantom in a contrast ratio of 2:1 between the activity concentrations of the sphere relative to the surrounding media. The phantom contained 0.5 mCi of ^{76}Br or 0.28 mCi of ^{18}F for the imaging session with this nuclide. The phantom was then scanned for a total of 60 min and sinograms were created for a number of frames with frame durations ranging from 10 s to 10 min. The frames duration and the injected amount of activity were chosen so that the same number of β^+ decay occurred during corresponding frames for ^{18}F and ^{76}Br . The noise in a region of interest (ROI) was measured in the sphere and in the uniform area by drawing a 6 mm ROI and extracting the standard deviation of the mean activity concentration within this ROI.

Figure 4 shows transaxial images of the phantom imaged with ^{18}F and ^{76}Br for a 30-s frame. We can note the obvious degradation of image quality by the increase noise in the ^{76}Br images, and also we can note that the MAP algorithm contributes largely at reducing the image noise. The contrast to noise ratio (CNR) calculated from the ratio of the measured activity concentration in the sphere relative to the activity concentration in the uniform area divided by the average noise in the sphere and in the uniform area is indicated on the figure. This CNR is observed to be lower for ^{76}Br and, furthermore, to be substantially higher for the MAP reconstructions. Higher CNR is

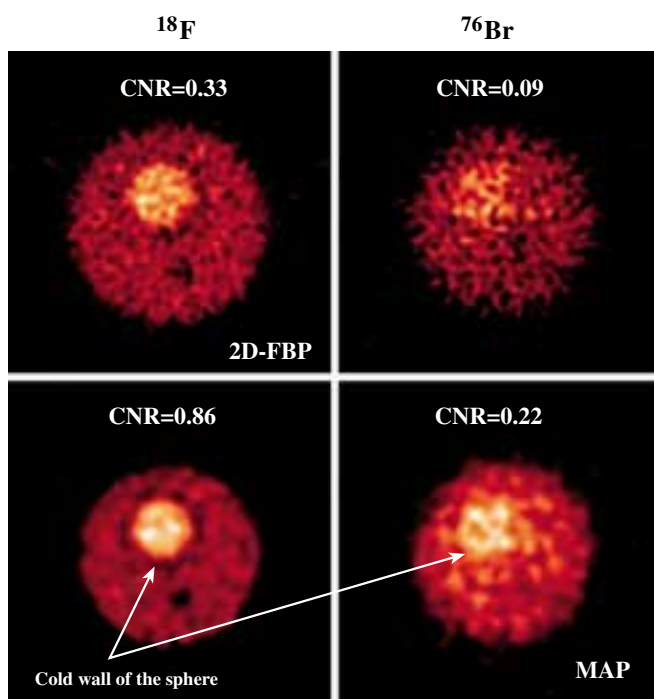


Figure 4.—Transverse slice of a phantom containing a sphere of 1 cm of diameter filled in a 2:1 ratio of activity concentration of the spheres relative to the surrounding area imaged in the micro-PET. Activity in ¹⁸F and ⁷⁶Br were chosen to provide the same number of decay during the 30 s frame duration for which this scan was performed. A notably increased noise can be observed in the ⁷⁶Br scan.

indicative of better image quality and increased detectability of features in images with lower statistics.

Figure 5 presents the relative average noise in the sphere plotted as function of the inverse of the square root of the frame duration for both nuclides and for images reconstruction using 2D-FBP and 3D-MAP. A linear relationship exists in accordance with the expected trend that the variance around the mean in a given uniform area should decrease linearly with the square of the frame duration. Two facts can be observed: 1) the relative noise of ¹⁸F is substantially less than the noise in ⁷⁶Br, and 2) the MAP algorithm, as visually assessed from the previous figure, provides lower noise values.

Imaging with ^{94m}Tc

Technetium-94m is produced from the irradiation by protons on a target of ⁹⁴MoO₃.^{9, 10} At end-of-bom-

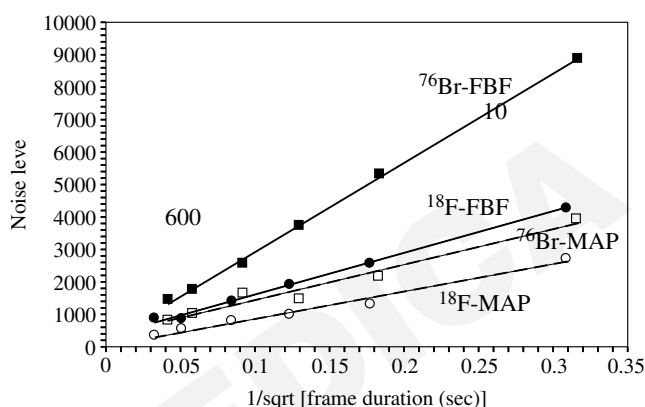


Figure 5.—Comparison of the noise level as a function of the scan duration in the micro-PET between ¹⁸F and ⁷⁶Br. The expected linear relationship with the square of the frame duration is observed. Maximum *a posteriori* performs substantially better at providing improved noise characteristics.

bardment, the number of nuclides in the respective metastable state (m) and ground state (g) states in ⁹⁴Tc are populated in approximately the same number. In terms of radioactivity, however, approximately 6% of the production goes to ^{94g}Tc states due to the respective half-lives of the m- relative to the g-state. Both isomers decay predominantly by positron emission to the 870 keV level in ⁹⁴Mo daughter with half-life of 52 and 250 min, respectively. Thus, when imaging by PET, the effective half-life of ^{94m}Tc will in fact be slightly longer. The measured activity of a radioactive source will thus be so that the proper decay correction function for this nuclide is thus:

$$A_m(t_0) = \frac{m(t)}{[B_m e^{(-\lambda_m t)} + F_g/F_m B_g e^{(-\lambda_g t)}]}$$

— where B_m and B_g are the β decay branching fractions for the m and g states (B_m=0.7 and B_g=0.2) and F_g and F_m are the fraction of produced activity (F_m=1, F_g=0.06).

It is important to consider the presence of ^{94g}Tc state since its relative importance relative to ^{94m}Tc increases over time and failure to account for this will result in inaccurate quantitation. A generalized formulation can be found in Smith *et al.*¹¹ for cases where other radioactive species are present. Quantitative imaging with this nuclide has also been studied by Barker *et al.*¹²

In Bigott *et al.*,⁹ we have shown that imaging a hot rod phantom results in the ability to identify 1.25 mm rods (separated by 6 mm) and that is better performed

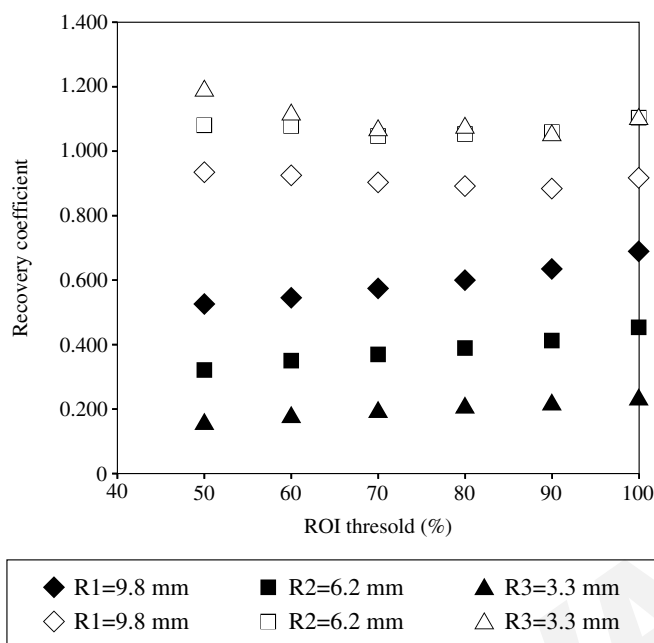


Figure 6.—Apparent recovery coefficients of spheres of diameter 3.9, 6.3, and 9.8 mm imaged in the micro-PET-F220 plotted as a function of the region of interest threshold (solid symbols) shows a linear relation with the threshold level and also shows very poor recovery values for this nuclide, even in the largest sphere. A partial volume correction based on the measured point spread function for this specific nuclide is shown to recover the activity in concentration in the spheres.

in a scanner capable of a better spatial resolution (micro-PET-R4 *vs* micro PET-F220). Also, it was shown that MAP reconstructions produce less noisy images and, thus, of higher contrast to noise values.

Similarly to the work done with ^{76}Br , the average activity concentrations in the spheres normalized by the expected activity concentration (defining the recovery coefficients) are plotted for the three sphere diameters in Figure 6 as a function of the ROI threshold. This figure indicates the poor performance of this nuclide to provide accurate quantitative measurements of the activity concentration due to the positron range. However, an accurate characterization of the point spread function allowed to correct the measured recovery coefficients and to accurately derive the true activity concentration in the spheres.

CASCADES SUBTRACTION

As mentioned before in this document, and reported elsewhere,^{5, 6, 12, 13} cascade γ rays create a back-

ground of counts in the projection space. Figure 7 shows a projection profile from a 3 cm diameter uniform phantom imaged with $^{94\text{m}}\text{Tc}$. The solid line indicates the measured coincidences corrected for the randoms while the dotted line represents this random profile. We can see that, outside of the phantom, an approximately uniform background of counts exists. The dashed line shows the profile of intensity through the same projection. We can see here that a simple scaling of the scatter function by any factor will not allow to get an accurate account for the counts outside the phantom. Alternatively, it was suggested that the randoms can be multiplied by an appropriate value such that the intensity of randoms added to the scatter distribution matches the measured projection tail. Although this can be done, we can see that substantial noise can be added in the process especially when the random rate is low (*i.e.* from low statistics or low counting rate scans). However, smoothing the randoms prior to adding the scatter component or the subtraction of a uniform distribution can provide an accurate subtraction of the cascade coincidences.

Imaging with ^{89}Zr

Figure 8 shows the hot rod Derenzo phantom imaged with several non-standard nuclides (^{61}Cu , ^{64}Cu , ^{76}Br , ^{86}Y , ^{89}Zr and ^{124}I) (as described before) and, for ^{89}Zr , the phantom images reveals that all the rods can be clearly identified even the 1 mm rods separated by 4 mm. This bears to the relatively low end-point energy of the positron extending up to 902 keV for an average energy of 395 keV owing to the fact that decay proceeds exclusively to the 909 keV level in ^{89}Y nucleus. This average energy is slightly larger than the 565 keV maximum positron energy from ^{18}F decay. Consequently, high images quality can be obtained with this nuclide. However, some considerations must be given to the 909 keV γ rays. This nuclide will thus have a much lower detection efficiency in the scintillator, thus the probability of cascades coincidences will be reduced, especially with lutetium oxyorthosilicate as the scintillator material. Moreover, attenuation or scatter of this γ ray in the animal will be low, especially in mouse studies, and as a such a small accumulation of cascade coincidences will be expected when imaging small animal with this nuclide. The same cannot be said, however, in human scanning as scatter within the patient will be large, thus reducing the energy of

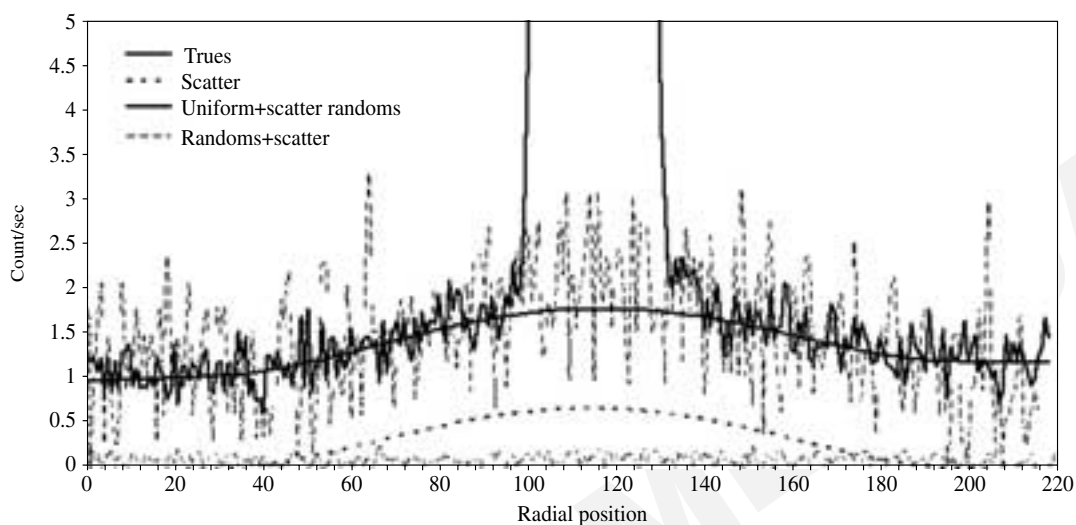


Figure 7.—Illustration of the cascades subtraction process on projection data acquired in the micro-PET-F220 with ^{94m}Tc . The trues coincidences (dark solid line) are composed of the sum of scatter (dash) and cascades (light solid line, uniform in the field-of-view for this phantom). Scaling the random coincidences (dot dash) and adding to the scatter (light dash line) is a process that adds considerable noise to the corrected sinogram.

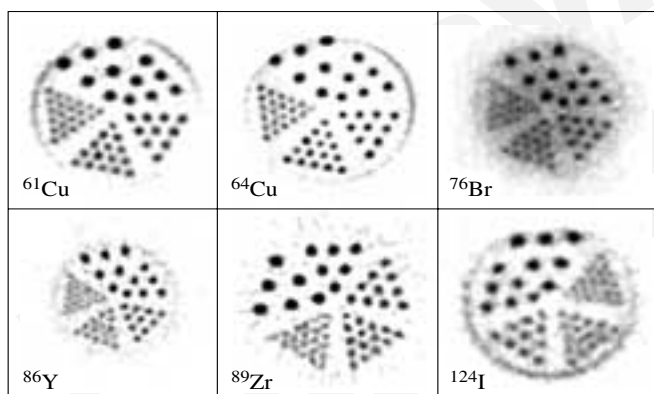


Figure 8.—Hot rod Derenzo phantom imaged with ^{61}Cu , ^{64}Cu , ^{76}Br , ^{86}Y , ^{89}Zr , ^{124}I . For ^{89}Zr imaging, all rods down to the 1 mm can be identified bearing to the relatively short range of the positrons. Images were reconstructed with 2D-filtered back-projection and no correction for the cascades was applied.

the γ ray energy to within the acceptance energy window of the scanner.

Discussion

We have presented data that illustrate that: 1) the positron range is clearly a detrimental factor in small animal PET imaging using non-standard nuclides; and 2) image noise is largely increased due to the range and

also due to the presence of cascades γ rays. Solutions for those problems exist in either using positron range correction built in the image reconstruction algorithm or by a detailed modeling of the system point spread function for each nuclide which in turn can be used in a postreconstruction image de-blurring process. The increase in noise in the images can in turn be compensated by the use of an appropriate statistical model in the image reconstruction such as in MAP.

The cascade γ rays also increases the detection burden from the camera detectors and thus one can expect that lower maximum activity can saturates the scanner or yield to inaccuracies in the camera deadtime correction model. The experiment reported in this document were performed at activities lower than any saturating level, but deadtime model inaccuracies must be kept in mind when imaging with large amount of activity. Thus, since image noise is larger, longer scanner times are required. From the data presented herein, it seems that scans three times longer with ^{76}Br relative to ^{18}F are required to obtain similar noise characteristics.

Conclusions

Non-standard nuclides are not particularly ideal for PET imaging due to the extended positron range and

to the sometimes numerous cascade ray emissions. However, high image quality and quantitation accuracy are possible when the positron range and the cascade γ rays are given special considerations. Imaging characterization must be done for each nuclide for a given scanner in order to ensure optimum image quality.

References

1. Schueller MJ, Mulnix TL, Jensen C, Holm S, Oakes TR, Roberts AD *et al.* Addressing the third gamma problem in PET. *IEEE Trans Nucl Science* 2003;50:50-2.
2. Welch MJ, Laforest R, Lewis JS. Production of non-standard PET radionuclides and the application of radiopharmaceuticals labeled with these nuclides. *Ernst Schering Res Found Workshop* 2007;p.159-81.
3. Ruangma A, Bai B, Lewis JS, Sun X, Welch MJ, Leahy R *et al.* Three-dimensional maximum a posteriori (MAP) imaging with radiopharmaceuticals labeled with three Cu radionuclides. *Nucl Med Biol* 2006;33:217-26.
4. Qi J, Leahy RM, Cherry SR, Chatzioannou A, Farquhar TH. High-Resolution 3D Bayesian image reconstruction using the microPET small-animal scanner. *Phys Med Biol* 1998;43:1001-13.
5. Beattie BJ, Finn RD, Rowland DJ, Pentlow KS. Quantitative imaging of bromine-76 and yttrium-86 with PET: a method for the removal of spurious activity introduced by cascade gamma rays. *Med Phys* 2003;30:2410-23.
6. Lubberink M, Schneider H, Bergstrom M, Lundqvist H. Quantitative imaging and correction for cascade gamma radiation of ^{76}Br with 2D and 3D PET. *Phys Med Biol* 2002;47:3519-34.
7. Nuclear Decay Data in the MIRD Format (NNDC) [homepage on the Internet]. Brookhaven National Laboratory. Available from: <http://www.nndc.bnl.gov/mird>.
8. Qaim SM, Bisinger T, Hilgers K, Nayak D, Coenen HH. Positron emission intensities in the decay of ^{64}Cu , ^{76}Br and ^{124}I . *Radiochim Acta* 2007;95:67-73.
9. Bigott HM, Laforest R, Liu X, Ruangma A, Wuest F, Welch MJ. Advances in the production, processing and microPET image quality of technetium-94m. *Nucl Med Biol* 2006;33:923-33.
10. Roesch F, Qaim SM. Nuclear data relevant to the production of the positron emitting technetium isotope $^{94\text{m}}\text{Tc}$ via the $^{94}\text{Mo}(p,n)$ -reaction. *Radiochim Acta* 1993;62:115-21.
11. Smith MF, Daube-Witherspoon ME, Plascjak PS, Szajek LP, Carson RE, Everett JR *et al.* Device-dependent activity estimation and decay correction of radionuclide mixtures with application to Tc-94m PET studies. *Med Phys* 2001;28:36-45.
12. Barker WC, Szajek LP, Green SL, Carson RE. Improved quantification for Tc-94m PET imaging. *IEEE Trans Nucl Science* 2001;48:739-42.
13. Herzog H, Tellmann L, Qaim SM, Spellerberg S, Schmid A, Coenen HH. PET quantitation and imaging of the non-pure positron-emitting iodine isotope ^{124}I . *Appl Radiat Isot* 2002;56:673-9.